Chromophore-Functionalized Glassy Polymers with Large Second-Order Nonlinear Optical Responses. Transient Dynamics and Local Microstructure of Poly(*p*-hydroxystyrenes) As Assessed by in-Situ Second Harmonic Generation Techniques

Millicent A. Firestone, Mark A. Ratner,* and Tobin J. Marks*

Department of Chemistry and the Materials Research Center, Northwestern University, Evanston, Illinois 60208-3113

Weiping Lin and George K. Wong

Department of Physics and Astronomy and the Materials Research Center, Northwestern University, Evanston, Illinois 60208-3113

Received September 29, 1994[⊗]

ABSTRACT: Microstructural relaxation of thin films of the poled, chromophore-functionalized amorphous polymer *N*-(4-nitrophenyl)-(*S*)-prolinoxypoly(*p*-hydroxystyrene) has been studied by *in-situ* second harmonic generation (SHG) techniques. The temporal and temperature dependence of the SHG intensity decay has been analyzed as a function of poling and processing parameters within the framework of the Kohlrausch–Williams–Watts (KWW "stretched exponential") model. The average SHG relaxation time, τ, increases rapidly upon reduction of the applied poling field strength, with increasing poling time (physical aging), and with decreasing film temperature. The other KWW parameter, β, which reflects the distribution of relaxation times, decreases (the distribution broadens) moderately with increases in the applied electric field strength and strongly with increases in poling time (physical aging). The observed value of β increases (the distribution narrows) with increasing film temperature. These trends and the variation in KWW parameters yield information regarding reorientation dynamics of the tethered chromophore molecules within the polymer matrix and thus on the nature of the system subspace which is explored during relaxation. Both parameters reveal a strikingly narrower distribution of relaxation times/reduced rotational mobility versus chromophore-doped, "guest–host" systems and classify the present materials as Angell "intermediate" glasses. The temperature dependence of the second harmonic signal decay after poling field cessation can be divided into two distinct regions: (i) above T_g, where the dynamics are characteristically nonlinear and best described by the Williams–Landel–Ferry (WLF) equation; (ii) below T_g, where the behavior is linear and modeled adequately by the Arrhenius equation. Analysis of the growth of the second harmonic signal as the poling field is applied yields a similar picture; however, limiting SHG values at temperatures significantly above T_g appear to be influenced by both thermal disruption of chromophore alignment and ion conduction/space charge effects.

In the accompanying paper,[1] we presented a systematic examination how polymer architectural characteristics and processing methodologies influence second-order nonlinear optical (NLO) response, and the temporal characteristics thereof, in a well-characterized, prototypical poled, chiral chromophore-functionalized glassy polymer, *N*-(4-nitrophenyl)-(*S*)-prolinoxypoly(*p*-hydroxystyrene) ((*S*)-NPP–PHS). In this paper, we extend this study with a detailed investigation of the effects of the electric field poling process, the procedure used to induce dipolar chromophore alignment essential for the observation of second-order NLO effects. Poled polymer systems are inherently thermodynamically unstable, the electric field-induced chromophore alignment representing an unstable ensemble. Hence, upon removal of the field, the aligned ensemble tends to undergo relaxation toward a more stable (random) configuration, thereby reducing (eventually to zero) the magnitude of the observed second-order optical nonlinearity. This temporal instability of the induced polar molecular orientation is a major obstacle to the realization of the technological potential of poled polymer films as efficient second-order NLO device materials. The mechanisms by which this relaxation process occurs are, in addition to being of technological significance, of fundamental scientific interest in understanding polymer chain dynamics.

To date, interest in NLO-active polymers at the fundamental macromolecular dynamics level has focused primarily on systems in which chromophores are doped into glassy polymer hosts as probes of local matrix reorientational dynamics.[2–7] Since it is essential that the probe molecules be truly monodispersed in the polymer matrix, molecular probe studies employing such doped ("guest–host") materials may not be as informative as those in which the probe is chemically bonded to the matrix (*i.e.*, to the polymer backbone).[8] Dynamics studies employing functionalized polymers have the attraction that selective attachment of the probe to various locations on the polymer backbone (*e.g.*, main chain vs side chain) is possible, thereby permitting identification of specific motions associated with various structural regions in the polymer. Until very recently, however, few polymer dynamic studies have focused on chromophore-functionalized NLO polymers.[9–14] Moreover, most of these studies have focused primarily on the temperature dependence of the NLO response.[9,10,12–14] To date, the principal poling technique has been corona poling,[9–12] which despite the attraction (as an alternative to contact poling) for inducing chromophore alignment, suffers from interpretive complications due to the

[⊗] Abstract published in *Advance ACS Abstracts,* February 15, 1995.

0024-9297/95/2228-2260$09.00/0

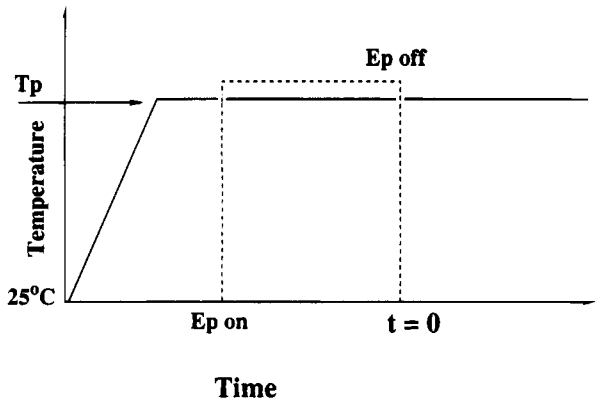

Figure 1. Timing cycle used for isothermal *in-situ* SHG poling studies.

unknown magnitudes of the electric fields involved and from currently unresolved issues concerning the magnitude of charge deposition and its subsequent decay.[15,16] These additional effects are difficult to separate from the fundamental process of interest—dipolar reorientation.[3,17]

In this paper, the relaxation behavior in a prototypical contact-poled, high-β chromophore-functionalized glassy polymer is examined using contact poling and *in-situ* second harmonic generation (SHG) measurement techniques. The time and temperature dependence of the SHG intensity as a function of poling conditions is examined in detail for (*S*)-NPP–PHS functionalized to varying levels with (*S*)-NPP.[1] An extensive data base is acquired and analyzed within the framework of the Kohlrausch–Williams–Watts formalism. The effects upon the response function of poling/processing parameters (*e.g.*, temperature, field strength, poling duration), each of which is independently varied, are examined. The results provide insight into means by which such materials could be improved for device applications and further demonstrate the attraction of *in-situ* SHG techniques to acquire fundamental information on amorphous polymer microstructure and dynamics.

Experimental Section

Preparation of Polymer Films. Poly(*p*-hydroxystyrene) (PHS) randomly functionalized with the chromophore *N*-(4-nitrophenyl)-(*S*)-prolinol (NPPOH), henceforth referred to as (*S*)-NPP–PHS, was synthesized as described in the accompanying paper[1] and characterized by standard analytical and spectroscopic methodologies. Glass transition temperatures, T_g, were determined by differential scanning calorimetry (Perkin-Elmer DSC-7, +10 °C/min heating rate) to be 134 and 146 °C for 36% and 12% (*S*)-NPP–PHS, respectively. Polymer films were fabricated and annealed as described previously.[1] Film thicknesses were determined with an α-step stylus profilometer (Tencor Instruments).

Contact Poling with in-Situ SHG Monitoring. The annealed (*S*)-NPP–PHS films were contact-poled *in situ* using the apparatus and configuration described in the accompanying paper.[1] The experiments examined the changes in the transient dynamics effected by selective modification of the electric-field poling parameters—applied field strength (E_p), duration of field application (t_{E_p}), and polymer film temperature (T). All of these studies were carried out isothermally (*i.e.*, maintaining the same temperature ±1 °C during poling and decay phases of the experiment) and using the timing cycle outlined in Figure 1. This procedure involves heating the polymer film to the desired poling temperature (T) and, after establishing thermal equilibrium, applying the electric field E_p. After completion of poling for a specific duration, t_{E_p}, the field is terminated while the film temperature is held constant.

Poling field strength (E_p) variation experiments were conducted in two poling field ranges: a low-field range (0.2–0.4 MV/cm) and a high-field range (1.0–1.2 MW/cm). The low-field data sets were collected isothermally at 133 °C using the methods outlined above. Samples were poled for 35 min (t_{E_p}) prior to field removal. High-field data were collected isothermally at 134 °C, the length of electric field application (t_{E_p}) being 15 min. The poling time was increased for the low-field set to allow sufficient chromophore orientation for obtaining a useful SHG signal-to-noise ratio during collection of the post-electric field data. SHG relaxation data collection began immediately upon field cessation ($t = 0$). Studies of electric field poling duration were carried out isothermally using the timing cycle detailed above (Figure 1). Two independent data sets were collected. In the first set, the impact of t_{E_p} on the recorded decay transients was examined by maintaining the film temperature at 130 °C (just below T_g) at a constant applied field strength of 1.1 MV/cm. The second set was collected at a film temperature of 110 °C (substantially below T_g) and a field strength of 0.4 MV/cm. The poling time, t_{E_p}, ranged from 10 to 40 min in both experiments. This range of times was selected to provide adequate SHG signal-to-noise ratios without requiring impractically long poling times. Extended contact poling, >45–60 min, invariably leads to dielectric breakdown of samples as indicated by rapid SHG fluctuations and/or an abrupt increase in current flow through the sample (greater than nanoamperes). Film breakdown is also evidenced in extreme cases by arcing between the electrodes and subsequent charring of the films.

To determine the effect of the film temperature on relaxation dynamics, the samples were maintained at the same temperature both during poling (SHG growth) and postpoling (SHG decay), while maintaining a constant applied field strength, E_p, and poling time, t_{E_p}. In these studies, both growth and decay of the second harmonic signal were measured for a range of temperatures between 120 and 135 °C. This range was selected since, at lower temperatures (<115 °C), insufficient initial chromophore orientation is observed, leading to poor second harmonic signal-to-noise ratios. At higher temperatures (>135 °C), the rate of second harmonic signal growth upon field application is too rapid to allow collection of an adequate data set. Data used for kinetic analyses of chromophore relaxation were collected over a wider range of sample temperature (115–153 °C). These latter studies were conducted isothermally and at constant field strength (1.25 MV/cm) and poling time (20 min).

Supplemental Corona Poling with in-Situ SHG Monitoring. Annealed (*S*)-NPP–PHS films were corona poled *in situ* using the apparatus and configuration described previously.[1] Corona poling was used to examine the relationship between maximum attainable second harmonic signal intensity and poling temperature. As noted above, corona poling provides an excellent complement to contact poling, since the former technique permits easy longer term monitoring of the signal under high-field conditions. Temperature-dependent studies were conducted isothermally on 12% functionalized (*S*)-NPP–PHS (T_g = 146 °C) using a corona voltage of +4.2 kV. Second harmonic data requisition began after 30 min of poling.

Second Harmonic Generation Measurements. Second harmonic generation measurements were carried out with a Q-switched Nd:YAG laser (Quanta-Ray, DCR-1) at 1.064 μm in the p–p polarized geometry. A quartz reference, which also monitors the laser power, and the sample were measured simultaneously throughout the course of each experiment. The instrumentation and calibration techniques are more fully described elsewhere.[1,19,20] Reproducibility in $I^{2\omega}$ measurements is estimated to be ±10%.

Data Analysis. Nonlinear least-squares analysis of the SHG intensity was performed using commercially available software (Kaleidagraph, Version 2.1, Synergy Software, Reading, PA). The best model is defined as that which best conforms by visual inspection to the experimental data, has the smallest numerical residual, and yields the smallest relative error for each of the fit parameters. The error limits established for each of the d_{33} data points were generally ±5%. For poled polymer films, the experimentally monitored SHG

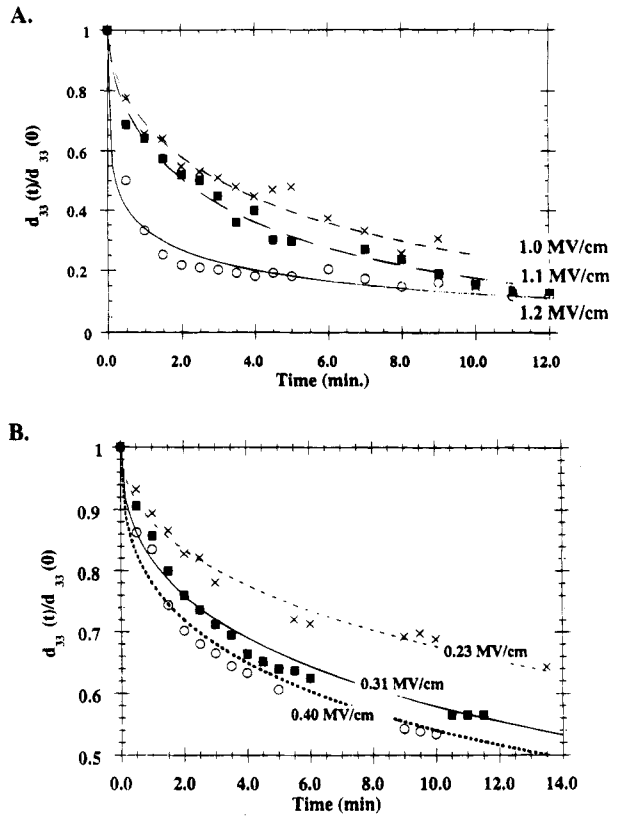

Figure 2. (A) Effect of applied contact poling field strength on the temporal characteristics of d_{33} for a 36% functionalized (*S*)-NPP–PHS film after cessation of poling. The electric field was terminated at $t = 0$ ($t_{E_p} = 15$ min; $T = 134$ °C). $E_p = 1.05$ MV/cm data are omitted for legibility. Lines through data points represent nonlinear least-squares fits to eq 2. (B) Effect of applied poling field strength on the temporal characteristics of d_{33} for a contact-poled 36% functionalized (*S*)-NPP–PHS film after cessation of poling. The electric field was terminated at $t = 0$ ($t_{E_p} = 35$ min; $T = 133$ °C). Lines through data points represent nonlinear least-squares fits to eq 2.

intensity normalized to unity at $t = 0$ is related to the second harmonic coefficient, via eq 1. Thus, either d_{33} or the second harmonic intensity can, in principle, be used in data analysis.

$$\frac{d_{33}(t)}{d_{33}(0)} = \left(\frac{I^{2\omega}(t)}{I^{2\omega}(0)}\right)^{1/2} \tag{1}$$

Results and Discussion

In this study, we analyze the temporal characteristics of the SHG intensity to quantify chromophore dipolar reorientation as a function of sample temperature, applied poling field strength, and duration of poling within the framework of the Kohlrausch–Williams–Watts (KWW) function and its description of the dynamics as a manifold of relaxation processes. Where appropriate, a biexponential function, with a "two-state" description of chromophore relaxation, is also examined, providing additional, complementary information regarding appended chromophore dynamics.

Effect of Poling Conditions on the Response Function. The effect of the applied field strength, E_p, on the SHG relaxation dynamics was investigated by contact poling 36% functionalized (*S*)-NPP–PHS (T_g = 134 °C) while maintaining both constant temperature (both during and after electric field cessation) and poling time, t_{E_p}. The relaxation transients obtained in these studies are shown in Figure 2. Qualitatively, it can be seen that relaxation is most rapid for samples poled at the highest field strengths, and the rate of second harmonic decay decreases at lower poling fields. Table 1 summarizes derived average relaxation times, τ, obtained by fitting the relaxation transients to the KWW function.

Table 1. Effect of Poling Field Strength, E_p, on Derived KWW Parameters for a 36% Functionalized (*S*)-NPP–PHS Film

E_p (MV/cm)	τ (min)	β
A. t_{E_p} = 15 min; Isothermal T = 134 °C		
1.00	5.88 (0.38)	0.59 (0.04)
1.05	4.72 (0.12)	0.58 (0.02)
1.10	3.98 (0.14)	0.59 (0.03)
1.20	0.76 (0.14)	0.28 (0.03)
B. t_{E_p} = 35 min; Isothermal T = 133 °C		
0.23	71.90 (3.10)	0.47 (0.04)
0.31	40.40 (1.90)	0.41 (0.04)
0.40	33.87 (2.00)	0.38 (0.03)

The relaxation dynamics (*i.e.*, dielectric response) of a wide variety of polymeric materials are found to exhibit the same nonexponential pattern of relaxation behavior,[21–29] described by the Kohlrausch–Williams–Watts (KWW) function[30,31] (eq 2). This function, some-

$$\phi(t) = e^{-(t/\tau)^{\beta}} \tag{2}$$

times referred to as a stretched exponential, can be understood in terms of a distribution of relaxation times, where ϕ represents the normalized relaxation function, τ represents the most probable relaxation time, and β is a constant between 0 and 1 which characterizes correlation effectiveness. Note that, as β decreases, the distribution broadens, incorporating a wider spectrum of relaxation times. Under certain conditions, β can equal unity, resulting in a single exponential, *i.e.*, characterized by a single relaxation time. Single-exponential (or Debye) relaxation has been shown to describe some materials, typically simple, non-glass-forming liquids. The vast majority of materials, however, do not conform to a single-exponential description,[32] since local structural variations on the microscopic level (*e.g.*, structural heterogeneities) tend to lead to a distribution of relaxation times. Thus, from a microstructural perspective, β can be related to disorder. It should be stressed, however, that the use of the KWW function to describe the relaxation process in these materials has no *a priori* theoretical justification.

As a generalization of Debye relaxation, monotonically decreasing data can be fit to any level of accuracy by a sum of exponential terms (eq 3).[33a] This is illustrated

$$\phi(t) = \sum_i w_i e^{-(t/\tau_i)} \tag{3}$$

in Figures 3 and 4, which present fits of the time-dependent second harmonic intensity data for a 36% functionalized (*S*)-NPP–PHS film, isothermally poled and then allowed to decay at $\sim T_g$. Visual comparison of the fits for $d_{33}(t)/d_{33}(0)$ to the KWW function (eq 2; Figure 3) and to a biexponential function (eq 3; Figure 4) shows that both functions afford equally convincing fits. Statistical comparison of the analyses shows that only a marginally significant improvement is obtained with the biexponential fit ($R = 0.997$ vs $R = 0.996$). This marginal improvement may be attributed to the increase in floating/fit parameters (3) available compared to the KWW function (2). This analysis shows that, in general, the KWW and biexponential fits cannot be distinguished at a statistically significant level.[33b]

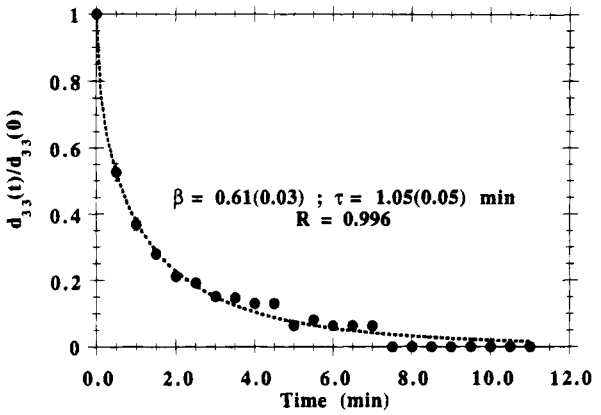

Figure 3. Temporal decay (after field cessation) characteristics of the second harmonic coefficient d_{33} for a contact-poled (T = 135 °C; t_{E_p} = 20 min; E_p = 1.25 MV/cm) 36% functionalized (*S*)-NPP–PHS film. The curve represents a nonlinear least-squares fit to the KWW function (eq 2).

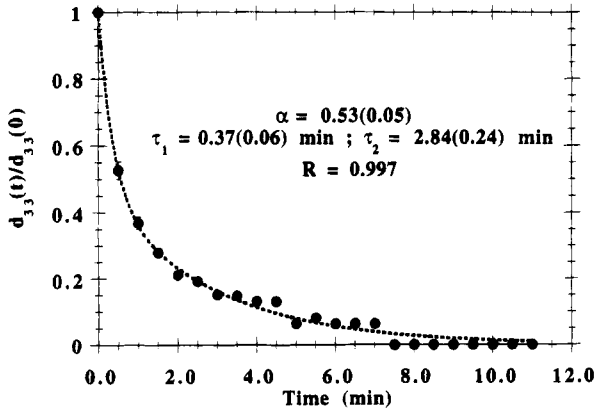

Figure 4. Temporal decay (after field cessation) characteristics of the second harmonic coefficient d_{33} for a contact-poled (T = 135 °C; t_{E_p} = 20 min; E_p = 1.25 MV/cm) 36% functionalized (*S*)-NPP–PHS film. The curve represents a nonlinear least-squares fit to the biexponential function (eq 3).

On a microscopic level, the observed decrease in relaxation time with poling field (Table 1) can be understood by considering the impact of a larger applied potential upon chromophore alignment. As the potential increases, the driving force to align the chromophores along the direction of the field increases, and a higher fraction of the chromophores are aligned. This, however, creates a thermodynamically unstable configuration such that, upon field termination, the systems furthest from thermodynamic equilibrium (*i.e.*, those samples poled with the highest field strength) relax most rapidly back to the stable configuration. Under these experimental conditions, β decreases with increasing field strength (Table 1). These trends indicate that, at higher applied field strengths, a wider range of relaxation times must be invoked to describe the decay process. This broadening of the relaxation time range at higher applied potentials may reflect the tendency of the chromophore substituents to access a larger dynamical range of barriers within the polymer matrix.

The effect of poling time, t_{E_p}, on (*S*)-NPP–PHS relaxation characteristics of the NLO chromophore was examined by isothermally contact poling a 36% functionalized film at constant field strength. The results (Figure 5) from isothermal annealing of the films in the presence of the electric field show that the decay rate is most rapid at short poling times, a trend observed

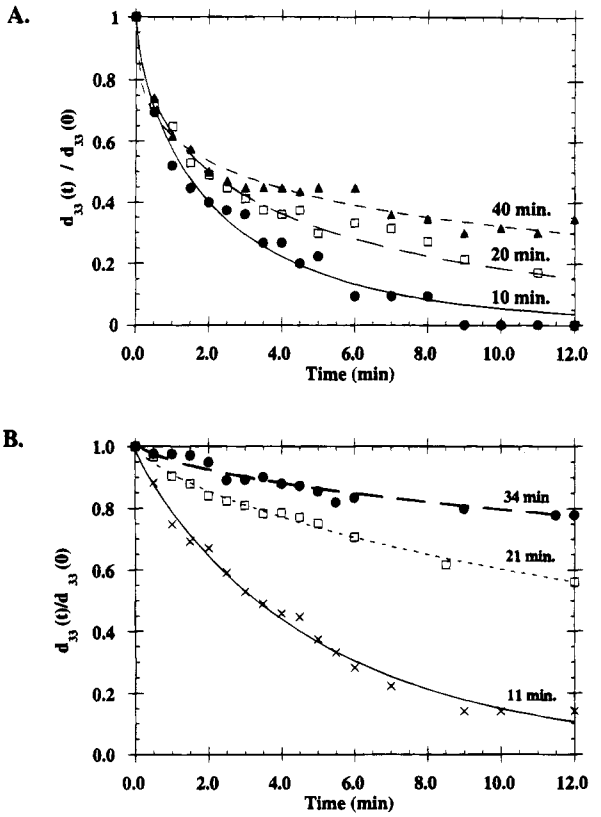

Figure 5. (A) Effect of poling time t_{E_p} (length of electric field application) on relaxation characteristics of d_{33} after cessation of poling. The electric field was terminated at t = 0. The study was performed on a contact-poled 36% functionalized (*S*)-NPP–PHS film (T = 130 °C; E_p = 1.1 MV/cm). Lines through data points represent nonlinear least-squares fits to eq 2. (B) Effect of poling time t_{E_p} (length of electric field application) on relaxation characteristics of d_{33} after cessation of poling. The electric field was terminated at t = 0. The study was performed on a contact-poled 36% functionalized (*S*)-NPP–PHS film (T = 110 °C; E_p = 0.4 MV/cm). Lines through data points represent nonlinear least-squares fits to eq 2.

Table 2. Effect of Poling Time, t_{E_p}, on KWW Fit Parameters for a 36% Functionalized (*S*)-NPP–PHS Film

poling time, t_{E_p} (min)	τ (min)	β
A. Isothermal T = 130 °C; E_p = 1.1 MV/cm		
10	2.33 (0.12)	0.73 (0.05)
20	3.95 (0.26)	0.56 (0.05)
40	7.00 (0.46)	0.36 (0.03)
B. Isothermal T = 110 °C; E_p = 0.40 MV/cm		
11	5.04(0.11)	0.93(0.04)
21	25.3(1.3)	0.73(0.02)
36	111.0(3.6)	0.58(0.01)

previously for several guest–host[2,34] systems and one chromophore-functionalized low-T_g methacrylate system.[11] This trend is further quantified by the average relaxation times, τ (Table 2), obtained by fitting the SHG intensity to the KWW function. At first glance, these results may seem to contradict those presented above, where the materials furthest from equilibrium (poled with the highest field strength) relax more quickly. Specifically, it might be anticipated that, in a kinetically-limited regime, increased poling time would produce a higher fraction of aligned chromophore moieties and, thus, a more thermodynamically unstable configuration which, in turn, would exhibit decreased relaxation times. However, physical aging, well-documented in glassy polymers,[35–37] must also be considered. The temperature range at which this generally occurs is

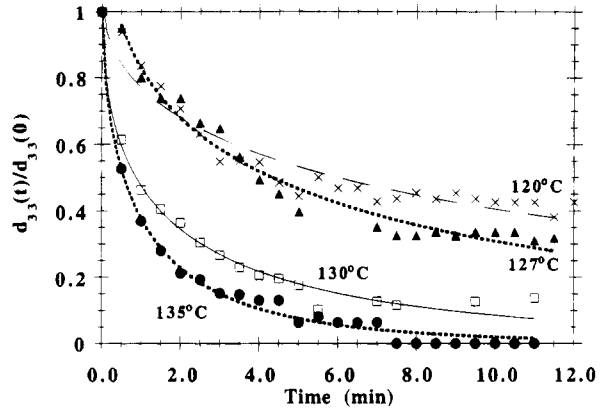

Figure 6. Second harmonic decay (after poling field termination at $t = 0$) transients for a 36% functionalized (*S*)-NPP–PHS film at a series of temperatures ($E_p = 1.25$ MV/cm; $t_{E_p} = 20$ min; poling temperature same as decay temperature). The 125 °C data are omitted for legibility. Lines through data points represent nonlinear least-squares fits to eq 2.

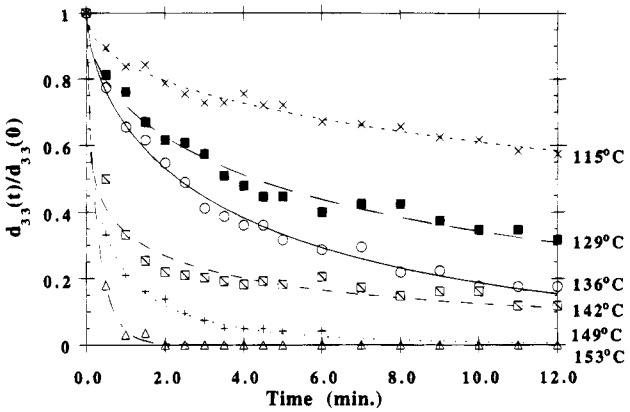

Figure 7. Second harmonic decay (after field removal at $t = 0$) transients for a 36% functionalized (*S*)-NPP–PHS film ($E_p = 1.1$ MV/cm; $t_{E_p} = 16$ min; constant temperature during both poling and decay) at a series of temperatures. The 134 °C data are omitted for legibility. Lines through data points represent nonlinear least-squares fits to eq 2.

bounded at the upper limit by T_g and at the lower by T_β, the highest secondary transition temperature—a range which encompasses the temperatures of the present studies. Physical aging primarily manifests itself in increasing relaxation times through a decrease or redistribution of the local free volume, thereby raising the barrier to dipole reorientation.[3b,10,11,29,38–40] Physical aging results in more efficient packing of the polymer chains, thereby decreasing chain mobility. If physical aging were important in (*S*)-NPP–PHS, the longer poling times would be expected to yield the slowest rates of SHG decay, as indeed observed.

As summarized in Table 2, β decreases with increasing poling time. This decrease implies that, at longer poling times, a broader distribution of relaxation times must be included to adequately describe the relaxation. Broadening of the relaxation time distribution as poling time is increased can again be attributed to the chromophore having the opportunity to explore a larger region or number of configurations within the polymer. Previous dielectric relaxation studies of β as a function of physical aging also demonstrated a decrease of β upon aging.[39] One previous SHG relaxation study employing extrinsic dye probes (guest–host systems) suggests that this trend may not obtain under conditions of more extensive aging (*i.e.*, at very long aging times) and at temperatures very far below T_g.[41]

The effect of sample temperature during poling and subsequent second harmonic decay (with constant E_p and t_{E_p}; shorter poling times at slightly lower fields allowed access to higher temperatures) was also investigated for (*S*)-NPP–PHS films (Figures 6 and 7). It is apparent that the data above T_g (134 °C) show more rapid decay than the sub-T_g trials (Figure 7). Examination of the average relaxation times, τ (Tables 3 and 4), for the full range of temperatures shows that, at the highest temperatures, the smallest average relaxation time constants are observed, while at temperatures below T_g, τ increases substantially. These results are consistent with the increased segmental mobility and local free volume expected at sample temperatures near T_g or above. This facilitates chromophore substituent reorientation upon removal of the applied field and rapid structural relaxation. These results underscore the significant microstructural/microdynamical changes occurring upon approaching the (*S*)-NPP–PHS glass transition region—rapidly decreasing viscosity and a concomitant increase in the rate of structural relaxation processes. The values of β_{decay} as a function of temperature are also presented in Table 3. Note that, as the glass transition region is approached, β increases, indicating that the distribution of relaxation times becomes narrower. The observed temperature dependence of β indicates that (*S*)-NPP–PHS is not thermorheologically simple; *i.e.*, the temperature dependence of $\phi(t)$ cannot simply be described as scaling of time by τ.[42,43]

Table 3. Effect of Film Temperature on the KWW Fit Parameters for a 36% Functionalized Film (*S*)-NPP–PHS ($E_p = 1.25$ MV/cm; $t_{E_p} = 20$ min)

temp (°C)	τ_{growth} (min)	β_{growth}	τ_{decay} (min)	β_{decay}
135	1.33 (0.06)	1.1 (0.08)	1.05 (0.05)	0.61 (0.03)
130	1.96 (0.09)	1.1 (0.09)	1.78 (0.02)	0.53 (0.02)
127	6.50 (0.65)	1.0 (0.1)	4.00 (1.5)	0.46 (0.02)
125	5.58 (0.20)	0.73 (0.03)	11.1 (0.82)	0.49 (0.03)
120	52.1 (5.3)	0.41 (0.02)	16.2 (0.48)	0.50 (0.02)

Table 4. SHG Decay Kinetic Data Collected for a 36% Functionalized (*S*)-NPP–PHS Film ($E_p = 1.1$ MV/cm; $t_{E_p} = 16$ min)

temp (°C)	τ^a (min)	k^b (min^{-1})
153	0.26 (0.02)	3.83
149	0.42 (0.02)	2.39
142	0.76 (0.16)	1.31
136	3.21 (0.10)	0.321
134	4.70 (0.28)	0.213
129	8.71 (0.41)	0.115
115	44.0 (1.4)	0.0227

[a] From fitting to KWW eq 2. [b] $k = \tau^{-1}$.

Much effort has been directed toward the study of the reorientation dynamics after electric field poling (SHG decay); however, few studies have examined the complementary transient orientation dynamics (chromophore alignment/SHG signal growth) immediately after application of a poling field.[3a,44,45] Furthermore, previous investigations presented only preliminary data analyses.[44,45] For this reason, a detailed investigation of (*S*)-NPP–PHS orientation dynamics was performed. A series of temperature-dependent SHG intensity growth profiles for isothermally poled, 36% functionalized (*S*)-NPP–PHS films are presented in Figure 8. When poling at temperatures near T_g (130 and 135 °C), rapid alignment of the chromophores in the electric field occurs until an asymptotic/steady-state region is reached. At temperatures further below T_g (*e.g.*, 120 °C), how-

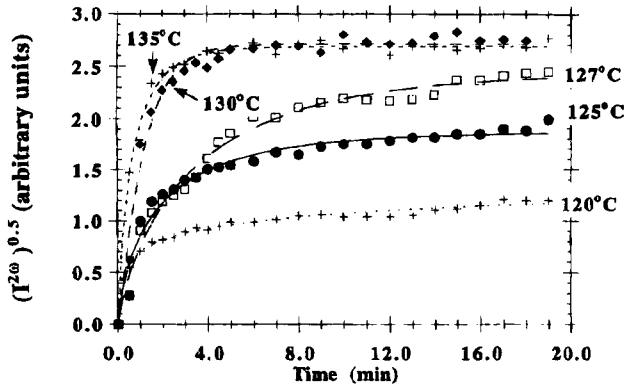

Figure 8. Second harmonic intensity growth curves for a 36% functionalized (*S*)-NPP–PHS film at a series of temperatures (E_p = 1.25 MV/cm; t_{E_p} = 20 min). The poling field was turned on at t = 0. Superimposed lines represent nonlinear least-squares fits of data to eq 4.

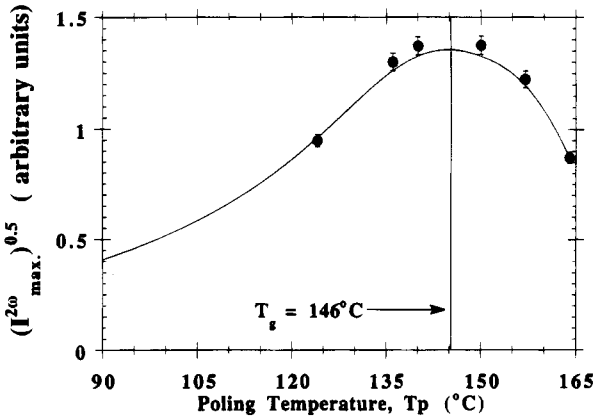

Figure 9. Temperature dependence of the limiting $(I^{2\omega})^{1/2}$ for a corona-poled (+4.2 kV; t_{E_p} = 30 min) 12% functionalized (*S*)-NPP–PHS film. The curve is drawn as a guide to the eye.

ever, a substantially reduced rate of alignment is observed. These trends can be quantified by fitting the temperature-dependent second harmonic intensity data to a modified KWW function (eq 4). The results of the

$$\phi(t) = 1 - e^{-(t/\tau)^{\beta}} \tag{4}$$

fit of the data to eq 4 are summarized and compared to the corresponding isothermal decay data in Table 3. Note that, for both decay and poling/growth trials (chromophore alignment), the average relaxation time increases with decreasing temperature, consistent with the concept of reduced dipolar mobility below T_g. This behavior indicates a major change in the appended chromophore local microenvironment, specifically, that a substantial increase in the barrier to rotation within the polymer matrix occurs in the glassy state. The movement of the chromophore is diminished as a consequence of reduction in both local free volume and polymer segmental mobility. As observed for both the decay mode and rise/growth mode SHG(t) measurements, β_{KWW} increases with increasing temperature. Note that this parameter appears to be significantly more temperature sensitive in the rise/growth data than in the corresponding decay results.

In addition to the polymer dynamic information in Figure 8, the magnitudes of the asymptotic SHG intensity values achieved also convey thermodynamic information. Assuming noninteracting chromophore dipoles, the "chromophore gas" model[46–48] predicts behavior of the second harmonic coefficient shown in eq 5 where $L_3(p)$ is the third-order Langevin function

$$d_{33} = \frac{1}{2} N f^{2\omega} f^{\omega} f^{\omega} \beta_{zzz} L_3(p) \tag{5}$$

with $p = f^{\omega}\mu E_p/kT$. From the slopes of the $d_{33}(t)$ plots in Figure 8, it can be seen that the 120–127 °C data are not at equilibrium after 20 min, while the data nearer to T_g (130 and 135 °C) appear to be asymptotic. In accord with eq 5, these curves exhibit limiting d_{33} values indistinguishable within expermimental error (±5%). Further studies of temperature effects on ultimate/equilibrium SHG responses were carried out for 12% functionalized (*S*)-NPP–PHS films using corona poling techniques. In contrast to contact poling, this method allows far higher excursions in temperature above T_g without dielectric breakdown. The results (Figure 9) show a peaking of d_{33} near T_g. The region below T_g can be interpreted as kinetically-limited chromophore orientation, with matrix mobility increasing as T_g is approached. At poling temperatures above T_g, d_{33} falls precipitously. This behavior is essentially reversible on lowering the temperature, and negligible film clouding or discoloration is observed which might be associated with sample degradation. While eq 5 predicts a decrease in d_{33} with increasing temperature, calculations using reasonable input parameters for eq 5 predict a decline in d_{33} from T = 146 → 165 °C of far less than the aforementioned experimental uncertainties (<5%). Although such behavior might reflect thermal disruption (beyond the thermodynamic $1/kT$ effects of eq 5) of cooperative chromophore alignment/acentric aggregates, the general absence of spectroscopic and SHG evidence for chromophore aggregation[1] argues against such microstructural behavior. Rather, we suggest that ion conduction/space charge effects, which are expected to increase significantly above T_g,[49] in combination with the behavior predicted by eq 5, account for the fall in d_{33} above T_g. Similar explanations have recently been advanced for guest–host systems.[5b,50] However, folded into the present dynamics picture must certainly be differences in rotational freedom of chromophores tethered to a polymer backbone vis-á-vis simple dissolved ones.

Temperature Dependence of the Response Function. The magnitudes and temperature dependence of the β and τ KWW parameters can be used to categorize different materials according to relaxation behavior. On the basis of an examination of a wide range of glass-forming materials, Angell has empirically classified them as strong, intermediate, or fragile.[43,51] "Strong" materials are typically network materials having three-dimensional structures (*e.g.*, SiO_2, GeO_2) and resistance to thermal degradation, reflected by very small changes in heat capacity (ΔC_p) through the T_g region. For strong materials, β exhibits a weak temperature dependence, generally ranging from 0.8 to 1.0. The other extreme, "fragile" materials, are liquids (*e.g.*, toluene) which characteristically do not possess specific bonding relationships other than generalized Coulombic or van der Waals interactions. The short-range structures of these materials are susceptible to changes in the T_g region, and they exhibit anomalously large ΔC_p values. For fragile materials, β is typically 0.3–0.5 and is strongly temperature-dependent around the transition region. Frequently, β decreases progressively with decreasing temperature. The "intermediate" classification encompasses a wide range of materials including alcohols and

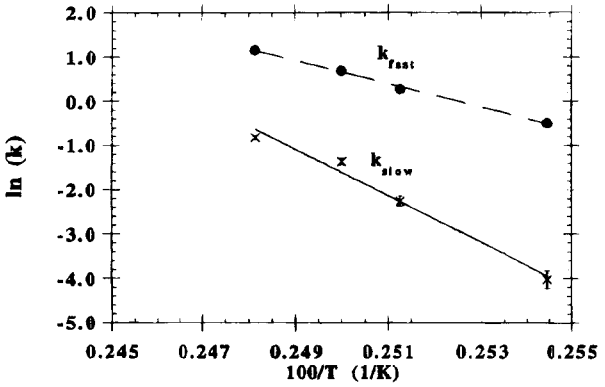

Figure 10. Arrhenius plot of fast (k_f) and slow (k_s) relaxation components of a contact-poled 36% functionalized (*S*)-NPP–PHS film below T_g (data from Figure 6).

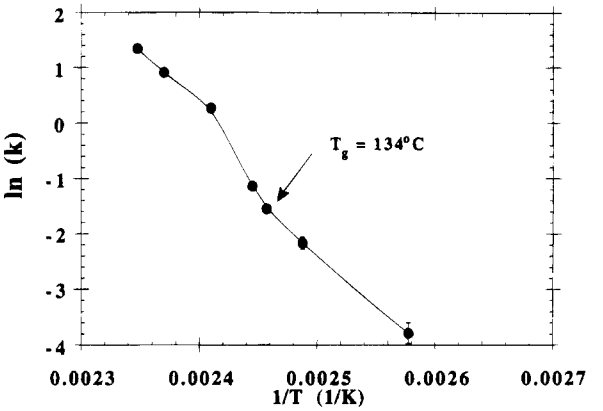

Figure 11. Arrhenius plot of the KWW-derived SHG decay rate constant data for a contact-poled 36% functionalized NPP–PHS film.

many amorphous polymers. In general, they possess some type of specific interactions such as hydrogen bonding or weak covalent interactions and exhibit many attributes of fragile materials, although the temperature dependence of β is somewhat less pronounced.

Examination of the isothermal decay curves for 36% functionalized (*S*)-NPP–PHS indicates that β (Table 3) exhibits some degree of temperature dependence, as expected for an intermediate material. Furthermore, the magnitude of β (0.5–0.6) in the temperature region studied and the observation of increasing β with increasing temperature correspond closely to the aforementioned intermediate classification. Note that these β values (0.5–0.6) are substantially greater than those reported in previous isothermal decay studies of guest–host materials,[3a,5b] indicating that a broader distribution of relaxation times exists in the doped materials compared to that found in the chromophore-functionalized polymers. The reduction in β (increased breath of distribution) likely reflects the increased rotational mobility inherent in guest–host materials.

A narrowing of the relaxation times distribution with increasing temperature (β approaching unity) has been interpreted, in a simple biexponential picture, as implying that the faster relaxation processes (τ_f) have smaller activation energies than the slower processes (τ_s).[52] Since the difference between τ_f and τ_s decreases with increasing temperature, a narrowing of the distribution is observed.[52,53] In other words, divergence of $1/\tau_f$ and $1/\tau_s$ as the temperature is lowered indicates a slowing of the relaxation modes involving diffusive motion and structural rearrangements relative to the fast relaxation processes. This divergence with decreasing temperature is illustrated for (*S*)-NPP–PHS films (poling and decay isothermally below T_g; Figure 6) in Figure 10, an Arrhenius plot of $1/\tau_f$ (k_f) and $1/\tau_s$ (k_s) data derived from nonlinear regression fitting to biexponential eq 6. Here

$$\phi(t) = c_f e^{-(t/\tau_f)} + c_s e^{-(t/\tau_s)} \tag{6}$$

c_f and c_s are coefficients describing the fractions of fast and slow kinetics. The empirical biexponential function has previously been applied to the study of polymer dynamics and can be viewed as a two-state description of chromophore reorientation rates, for example, those occurring in "liquid-like" and "glass-like" regions of the polymer matrix.[54,55]

Since the temperature-dependent behavior of the sub-T_g relaxation processes for (*S*)-NPP–PHS is Arrhenius-like (eq 7), temperature-independent activation energies, E_a, for the fast and slow processes can be determined. The faster relaxation process yields an activation energy of 52.5 ± 5.3 kcal/mol. The activation energy associated with the slow relaxation processes is nearly twice that of the fast process, 104.6 ± 10.4 kcal/mol. The exponential dependence of the relaxation

$$\tau = \tau_0 e^{E_a/RT} \tag{7}$$

times on temperature below T_g suggests that the observed mobility is noncooperative in nature (*i.e.*, does not involve participation of a large region of the polymer) but rather is due to local mode relaxations involving rotations of the individual chromophoric units or other functional group motion.[56,57] The magnitude of each of the activation energies is larger than that found in recent studies of the lower T_g polymers spiropyran-modified poly(L-lysine)[58] and (dimethylamino)nitrostilbene-substituted poly(butyl methacrylate).[59] The larger apparent activation energies for (*S*)-NPP–PHS are consistent with the higher T_g and the slower observed rate of SHG decay subsequent to poling field removal. The activation energy corresponding to the slow process, however, is only slightly higher than that reported for a DANS-functionalized side-chain polymer, which possesses approximately the same T_g.[60]

Like β, the KWW τ can also be used to categorize glass-forming materials according to Angell's classification. Strong materials usually have an Arrhenius temperature dependence (eq 7), with large but temperature-independent activation energies. Fragile materials exhibit two Arrhenius regions, one at high temperatures ($T \gg T_g$) with a lower activation energy than usually found in strong materials and a second region at low temperatures with a very large E_a. The two Arrhenius regions are connected by a region of strong curvature, with E_a monotonically increasing as temperature decreases. Intermediate materials show many aspects of fragile behavior but exhibit a slightly less pronounced temperature dependence of the effective E_a. The temperature dependence of SHG decay through a full range of temperatures above and below the glass transition temperature for 36% functionalized (*S*)-NPP–PHS is presented in Figure 11 (Table 4). The semilog plot of the relaxation time constant, k ($k = 1/\tau$), as a function of $1/T$ confirms approximately linear behavior below T_g (134 °C) and the Arrhenius temperature dependence of τ. At higher temperatures, however, curvature is evident, again suggesting intermediate behavior. The temperature dependence of polymer glass relaxation times in fragile and intermediate materials above T_g is

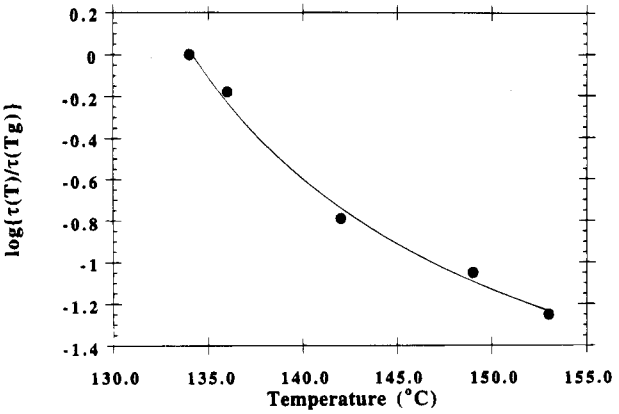

Figure 12. Temperature dependence of the SHG relaxation time constant, τ, for a 36% functionalized (*S*)-NPP–PHS film above T_g. The solid curve represents a nonlinear least-squares fit to the WLF equation (eq 8 where $C_1 = 2.35$, $C_2 = 17.02$ K, and $T_g = 134.2$ °C).

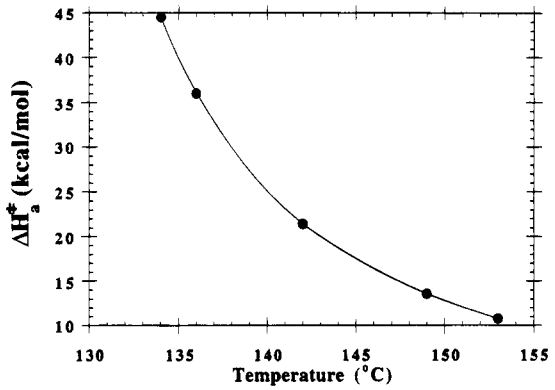

Figure 13. Activation enthalpy data as a function of temperature from above-T_g SHG relaxation data on a 36% functionalized (*S*)-NPP–PHS film. The curve is drawn as a guide to the eye.

often described by the Williams–Landel–Ferry (WLF) function[61] (eq 8) where a_T is the ratio of the relaxation

$$\log a_T = \frac{-C_1(T - T_g)}{C_2 + T - T_g} \tag{8}$$

times (obtained by fitting to the KWW function) at temperature T to that at the glass transition temperature, T_g. C_1 and C_2 are empirical constants which depend strongly on the polymer.[62] Since the WLF equation is only valid above T_g (due to its inability to accurately account for the nonequilibrium state of the glass), the present analysis is applied only to the relaxation transients collected $T \geq T_g$ for 36% functionalized (*S*)-NPP–PHS (Figure 7 and Table 4). The WLF parameters obtained (Figure 12) are $C_1 = 2.35$ and $C_2 = 17.02$ K. The success of modeling the above-T_g relaxation dynamics with the WLF expression has been suggested to indicate that at these temperatures ($T > T_g$) the relaxation mechanism becomes more cooperative, involving the participation of larger regions of the polymer chain(s).[28]

From the WLF equation, an apparent activation enthalpy for relaxation above T_g can be derived (eq 9),[62,63] where R is the ideal gas constant. $\Delta H_a^{\ddagger}$ is not

$$\Delta H_a^{\ddagger} = \frac{RC_1C_2T^2}{(C_2 + T - T_g)^2} \tag{9}$$

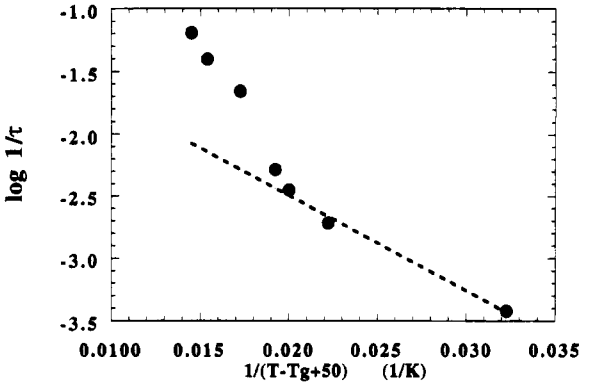

Figure 14. VTF plot of SHG relaxation data for a contact-poled 36% functionalized (*S*)-NPP–PHS film. The dashed line represents a linear least-squares fit of sub-T_g data.

temperature-independent but rather increases rapidly with decreasing temperature (Figure 13), ranging from ~11 kcal/mol at 153 °C to ~45 kcal/mol at 134 °C. This trend is due to the onset of rotational and translational motion that was prohibited in the structurally arrested glassy state. From Dhinojwala *et al.*'s[5] WLF plot for the temperature-dependent behavior of a DANS-doped glassy polymer (PIBM) the $\Delta H_a^{\ddagger}$ above T_g can be estimated to be ~1 kcal/mol, a value substantially less than that found in the present study. The smaller activation energy found for the doped polymers compares favorably with activation energies typically found for small penetrant molecules diffusing through amorphous polymer matrices.[64]

The temperature dependence of τ for (*S*)-NPP–PHS can also be examined by replotting the relaxation data using the Vogel–Tamann–Fulcher (VTF) equation[65–67]—a WLF equivalent function (eq 10) where τ is

$$\tau(T) = A \exp\left(\frac{-B}{T_0 - T}\right) \tag{10}$$

the KWW-derived relaxation time, A and B are system-dependent constants, and T_0 is a reference temperature, typically 50 °C below T_g. The results of this analysis (Figure 14) compare favorably with those recently reported for two chromophore-functionalized PMMA polymers.[6,68,69] Note that one analysis[68] used a modified VTF function which extends the validity of eq 10 to temperatures below T_g, since the majority of the relaxation data were recorded in that region. The chromophore-functionalized PMMA polymers[68,69] also exhibited a discontinuity in VTF plots (*i.e.*, change in slope) as observed for (*S*)-NPP–PHS (Figure 14). The temperature at which this discontinuity occurs has been termed the critical temperature, T_c.[65–67] For (*S*)-NPP–PHS, this temperature corresponds closely to the glass transition temperature. The lesser slope at temperatures below T_g indicates that, in this region, the relaxation processes are not as thermally sensitive as at higher temperatures. Thus, the system is more stable below T_g. In contrast, the PMMA polymers examined by Burland *et al.*[68,69] exhibit T_c at ~50 °C below T_g, indicating a significant difference in the relaxation behavior of the two systems; a 50 °C difference between T_g and T_0 is typical of many structural polymers.[65–67] This result indicates that (*S*)-NPP–PHS is more orientationally stable than the functionalized PMMA polymers since, for the latter, the onset of enhanced thermal stability does not appear until the temperature is reduced to ~50 °C below T_g. One

possible explanation for the enhanced stability of (*S*)-NPP–PHS is the stiffer backbone and presence of secondary bonding interactions such as hydrogen bonding.

Conclusions

The results of this study demonstrate that *in-situ* SHG measurements provide an incisive method for probing polymer dynamics and local polymer microstructure. By analyzing relaxation transients during and after poling, while systematically varying selected poling/processing parameters such as duration of poling, temperature, and applied field strength, information regarding the rotational dynamics and local microstructure of the appended chromophore can be obtained. Data analysis using the empirical KWW function and the associated fit parameters for (*S*)-NPP–PHS shows that τ increases substantially upon reduction of the applied poling field strength, with increasing poling time (physical aging) and with a decrease in sample temperature. The distribution broadens (β decreases) moderately with an increase in the applied field strength and sharply with increased poling time. This broadening of the relaxation time distribution can be attributed to the tendency of the pendant chromophore units to access a larger dynamic range of barriers within the polymer. Conversely, β increases (the distribution narrows) with increasing film temperature, attributable to increased cooperativity of motion within the polymer matrix. The majority of observed β values in this study fall within the range of 0.5–0.6—values typically encountered in studies of relaxation behavior in both organic and inorganic glasses subjected to electrical, mechanical, or thermodynamic stresses.[1,29,57,70]

The temperature dependence of τ can be divided into two distinct regions: sub-T_g, where the dynamics can be adequately modeled using the Arrhenius equation, and above-T_g, where the behavior can be described by the Williams–Landel–Ferry (WLF) or the equivalent Vogel–Tamman–Fulcher (VTF) function. Examination of the VTF plot for the KWW relaxation times of (*S*)-NPP–PHS films reveals a change in slope at T_g, signaling a change in the thermal sensitivity of the polymer matrix. A recent, similar analysis of two functionalized PMMA polymers revealed a similar discontinuity in the VTF plot; however, the location was substantially below T_g (T_g – 50 °C). Thus, the (*S*)-NPP–PHS system is more stable, due presumably to a less mobile architecture and secondary bonding interactions. In marked contrast, the majority of WLF and VTF plots for guest–host NLO polymers do not appear to exhibit such a slope discontinuity and are essentially linear.[68,69] This differing behavior is likely due to the lack of strong correlations between the chromophore probe dynamics and the dynamics of the host polymer. In other words, the temperature-dependent behavior of the chromophore dopants is far less sensitive to changes in the host polymer dynamics near T_g, since the chromophore units reside in voids between polymer chains and are not directly coupled to the motion of the polymer. Further experiments on different types of side-chain and host–guest NLO polymers are needed to assess the generality of these conclusions. Evaluation of the temperature-dependent (*S*)-NPP–PHS SHG relaxation data using the WLF equation affords a range of activation enthalpies, which are found to increase as T_g is approached (10.8–44.5 kcal/mol). These values are ~10× greater than those found for simple guest–host PMMA systems.

The growth (field-on) dynamics of the temperature-dependent (*S*)-NPP–PHS SHG signal were also examined using the KWW function. As was the case for the SHG decay, the KWW τ parameter decreases with increasing sample temperature. The width of the distribution, β, approaches unity with increasing temperature, implying that a single alignment mechanism (electric field biasing of the chromophore dipoles) dominates at these temperatures. The distribution broadens at lower temperatures, presumably incorporating additional alignment mechanisms, such as side-chain motion coupled with main-chain reorganizational motion. While we have provided qualitative explanations for many of the observed changes in the fit parameters, further interpretation awaits an appropriate theoretical analysis. This will be presented in a subsequent contribution.[70]

Acknowledgment. We thank NSF (Grant DMR 9120521 through Northwestern University Materials Research Center) and AFOSR (Contract 93-1-0114) for support of this research. M.A.F. thanks IBM for a Predoctoral Fellowship.

References and Notes

(1) Firestone, M. A.; Park, J.; Minami, N.; Ratner, M. A.; Marks, T. J.; Lin, W.; Wong, G. K. *Macromolecules* **1995**, *28*, 2247–2259.
(2) (a) Burland, D. M.; Miller, R. D.; Walsh, C. A. In *Optical Nonlinearities in Chemistry*; Burland, D. M., Ed.; *Chem. Rev.* **1994**, *94*, 31–75 and references therein. (b) Marks, T. J.; Ratner, M. A. *Angew. Chem.*, in press.
(3) (a) Dhinojwala, A.; Wong, G. K.; Torkelson, J. M. *Macromolecules* **1992**, *25*, 7395–7397. (b) Hampsch, H. L.; Yang, J.; Wong, G. K.; Torkelson, J. M. *Macromolecules* **1990**, *23*, 3640–3647, 3648–3654.
(4) (a) Mortazavi, M. A.; Knoesen, A.; Kowel, S. T.; Higgins, B. G.; Dienes, A. *J. Opt. Soc. Am. B* **1989**, *6*, 733–741. (b) Mortazavi, M. A.; Knoesen, A.; Kowel, S. T.; Henry, R. A.; Hoover, J. M.; Lindsay, G. A. *Appl. Phys. B* **1991**, 287–295.
(5) (a) Boyd, G. T.; Francis, C. V.; Tend, J. E.; Ender, D. A. *J. Opt. Soc. Am. B* **1991**, *8*, 887–894. (b) Singer, K. D.; King, L. A. *J. Appl. Phys.* **1991**, *70*, 3251–3255. (c) Boyd, G. T. *Thin Solid Films* **1987**, *152*, 295–304.
(6) (a) Valley, J. F.; Wu, J. W.; Ermer, S.; Stiller, M.; Binkley, E. S.; Kenney, J. T.; Lipscomb, Lytel, R. *Appl. Phys. Lett.* **1992**, *60*, 160–162. (b) Wu, J. W.; Valley, J. F.; Stiller, M.; Ermer, S.; Binkley, E. S.; Kenney, J. T.; Lipscomb, Lytel, R. *SPIE Proc.* **1991**, *1560*, 196–205. (c) Wu, J. W.; Binkley, E. S.; Kenney, J. T.; Lytel, R.; Garito, A. F. *J. Appl. Phys.* **1991**, *69*, 7366–7368.
(7) (a) Stahelin, M.; Burland, D. M.; Ebert, M.; Miller, R. D.; Smith, B. A.; Tweig, R. J.; Voksen, W.; Walsh, C. A. *Appl. Phys. Lett.* **1992**, *61*, 1626–1628. (b) Schüssler, S.; Richert, R.; Bässler, H. *Macromolecules* **1994**, *27*, 4318–4326.
(8) Law, K. Y.; Loufty, R. O. *Macromolecules* **1981**, *14*, 587–591.
(9) (a) Jungbauer, D.; Teraoka, I.; Yoon, D. Y.; Reck, B.; Swalen, J. D.; Tweig, R.; Willson, G. C. *J. Appl. Phys.* **1991**, *69*, 8011–8017. (b) Eich, M.; Sen, A.; Looser, H.; Bjorklund, G. C.; Swalen, J. D.; Tweig, R.; Yoon, D. Y. *J. Appl. Phys.* **1989**, *66*, 2559–2567. (c) Teraoka, I.; Jungbauer, D.; Reck, B.; Yoon, D. Y.; Tweig, R.; Willson, C. G. *J. Appl. Phys.* **1991**, *69*, 2568–2576.
(10) (a) Köhler, W.; Robello, D. R.; Willand, C. S.; Williams, D. J. *Macromolecules* **1991**, *24*, 4689–4599. (b) Köhler, W.; Robello, D. R.; Dao, P. T.; Willand, C. S.; Willams, D. J. *J. Phys. Chem.* **1991**, *93*, 9157–9166.
(11) Lindsay, G. A.; Henry, R. A.; Hoover, J. M.; Knoesen, A.; Mortazavi, M. *Macromolecules* **1992**, *25*, 4888–4894.
(12) Man, H. T.; Yoon, H. N. *Adv. Mater.* **1992**, *4*, 159–168.
(13) (a) Ye, C.; Minami, N.; Marks, T. J.; Yang, J.; Wong, G. K. *Macromolecules* **1988**, *21*, 2899–2901. (b) Dai, D. R.; Marks, T. J.; Yang, J.; Lundquist, P. M.; Wong, G. K. *Macromolecules* **1990**, *23*, 1891–1894. (c) Jin, Y.; Carr, S. H.; Marks, T. J.; Lin, W.; Wong, G. K. *Macromolecules* **1992**, *4*, 963–965.
(14) Wang, H.; Jarnagin, R. A.; Samulski, E. T. *Macromolecules* **1994**, *27*, 4705–4713.
(15) Deposited charge (presumably as cation-radical structures) can contribute to the measured SHG via a dc field-induced γ

term. The magnitude will vary with the chromophore second hyperpolarizability and the applied field; it will decay as the stored charge decays. The contribution of this term to $\chi^{(2)}$ immediately prior to cessation of poling has been found to vary from ≲5% in chromophore-like NPP[1,16] to the 18–20% range for very high-γ chromophores.[2,3,5a]

(16) Firestone, M. A.; Marks, T. J., unpublished results.
(17) (a) Hampsch, H. L.; Torkelson, J. M.; Bethke, S. J.; Grubbe, G. *Polym. Prepr. (Am. Chem. Soc., Div. Polym. Chem.)* **1990**, *31*, 373, 374. (b) Haber, K. S.; Ostrowski, M. H.; O'Sickely, M. J.; Lackritz, H. S. *Mater. Res. Soc. Symp. Proc.* **1994**, *328*, 595–600.
(18) Firestone, M. A.; Park, J.; Marks, T. J.; Ratner, M. A.; Lin, W.; Wong, G. K., manuscript in preparation.
(19) Ye, C.; Marks, T. J.; Yang, J.; Wong, G. K. *Macromolecules* **1987**, *20*, 2322–2324.
(20) Ye, C.; Minami, N.; Marks, T. J.; Yang, J.; Wong, G. K. *Macromolecules* **1988**, *21*, 2899–2901.
(21) Jonscher, A. K. *Nature* **1977**, *267*, 673–679.
(22) Shlesinger, M. F.; Montroll, E. W. *Proc. Natl. Acad. Sci. U.S.A.* **1984**, *81*, 1280–1283.
(23) Jonscher, A. K. In *Physics of Thin Films*; Hass, G., Francome, M. H., Eds.; Academic Press: New York, 1980; Vol. II; pp 205–273.
(24) (a) Ngai, K. L.; Yee, A. F. In *Relaxation in Complex Systems*; Ngai, K. L., Wright, G. B., Eds.; Naval Research Laboratory and Office of Naval Research: Arlington, VA, 1984; pp 145–165. (b) Rendell, R. W.; Ngai, K. L. In *Relaxation in Complex Systems*; Ngai, K. L., Wright, G. B., Eds.; Naval Research Laboratory and Office of Naval Research: Arlington, VA, 1984; pp 309–345.
(25) Jonscher, A. K. *IEEE Trans. Electr. Insul.* **1992**, *27*, 407–423.
(26) Scher, H.; Schlesinger, M. F.; Bendler, J. T. *Phys. Today* **1991**, *44*, 26–34.
(27) Frauenfelder, H.; Sligar, S. G.; Wolynes, P. G. *Science* **1991**, *254*, 1598–1603.
(28) Williams, G. *J. Non-Cryst. Solids* **1991**, *131–133*, 1–12.
(29) Etienne, S.; Cavaille, J. Y.; Perez, J. *J. Non-Cryst. Solids* **1991**, *131–133*, 60–70.
(30) Kohlrausch, R. *Ann. Phys. (Leipzig)* **1847**, *12*, 393–395.
(31) Williams, G.; Watts, D. C. *Trans. Faraday Soc.* **1970**, *66*, 80–85.
(32) (a) Ngai, K. L. *Comments Solid State Phys.* **1979**, *9*, 127–139. (b) Klafter, J.; Drake, J. M. In *Dynamics and Mechanisms of Photoinduced Transfer*; Mataga, N., Okada, T., Matsubata, H., Eds.; Elsevier: Amsterdam, The Netherlands, 1992; pp 345–355.
(33) (a) Scherer, G. W. *Relaxation in Glass and Composites*; John Wiley & Sons: New York, 1986; pp 41–45. (b) Marshall, D. B. *Anal. Chem.* **1989**, *61*, 660–667.
(34) Lee, S. C.; Kidoguchi, A.; Watanabe, T.; Yamamoto, H.; Hosomi, T.; Miyata, S. *Polym. J.* **1991**, *23*, 1209–1212.
(35) Struik, L. C. E. *Ann. N.Y. Acad. Sci.* **1976**, *279*, 78–85.
(36) Struik, L. C. E. *Physical Aging in Amorphous Polymers and Other Materials*; Elsevier: Amsterdam, The Netherlands, 1978.
(37) Aklonis, J. J. *Polym. Eng. Sci.* **1981**, *21*, 896–902.
(38) Greiner, R.; Schwarzl, F. R. *Rheol. Acta* **1984**, *32*, 378–395.
(39) Alegria, A.; Goitiardia, L.; Telleria, I.; Colmenero, J. *J. Non-Cryst. Solids* **1991**, *131–133*, 457–461.
(40) (a) Schlosser, E.; Schonhals, A. *Polymer* **1991**, *32*, 2135–2139. (b) Royal, J. S.; Torkelson, J. M. *Macromolecules* **1993**, *26*, 5331–5335.
(41) Hampsch, H. L.; Torkelson, J. M.; Yang, J.; Wong, G. K. *Polym. Commun.* **1989**, *30*, 40–43.
(42) Rekhson, S. *J. Non-Cryst. Solids* **1987**, *95–96*, 131–148.
(43) Fredicksen, G. H. *Ann. Rev. Phys. Chem.* **1988**, *39*, 149–180.
(44) Dhinojwala, A.; Royal, J. S.; Wong, G. K.; Torkelson, J. M. *Polym. Prepr. (Am. Chem. Soc., Div. Polym. Chem.)* **1992**, *33*, 107, 108.
(45) Cheng, L.-T.; Foss, R. P.; Meredith, G. R.; Tam, W.; Zumsteg, F. C. *Mater. Res. Soc. Symp. Proc.* **1992**, *247*, 27–38.
(46) Meredeth, G. R.; Van Dusen, J. G.; Williams, D. J. *Macromolecules* **1982**, *15*, 1385–1389.
(47) Singer, K. D.; Sohn, J. E.; Lalama, S. J. *J. Appl. Phys. Lett.* **1986**, *49*, 248–250.
(48) Singer, K. D.; Kuzyk, M. G.; Sohn, J. E. *J. Opt. Soc. Am. B* **1987**, *4*, 968–975.
(49) Van Turnhout, J. *Thermally Stimulated Discharge of Polymer Electrets*; Elsevier: Amsterdam, The Netherlands, 1975.
(50) (a) Esselin, S.; LeBarney, P.; Broussoux, D.; Dubois, J. C.; Raffy, J.; Pochelle, J. P. *SPIE Proc.* **1988**, *971*, 159–168. (b) Schüssler, S.; Richert, R.; Bässler, H. *Macromolecules* **1994**, *27*, 4318–4326.
(51) (a) Angell, C. A. *Relaxations in Complex Systems*; Office of Naval Research: Arlington, VA, 1984; pp 3–12. (b) Angell, C. A. *J. Non-Cryst. Solids* **1991**, *131–133*, 13–31.
(52) Tauke, J. T.; Litovits, A.; Macedo, P. B. *J. Am. Ceram. Soc.* **1968**, *51*, 158–163.
(53) Jackle, J. *Rep. Prog. Phys.* **1986**, *49*, 171–231.
(54) Yu, W. C.; Chong, S. P. S.; Roberston, R. E. *Macromolecules* **1988**, *21*, 355–364.
(55) Rossler, E.; Sillescu, B. In *A Comprehensive Treatment: Glass and Amorphous Materials*; VCH: Weinheim, FRG, 1991; Vol. 9, pp 574–615.
(56) Robert, G. E.; White, E. F. T. In *The Physics of Glassy Polymers*, 1st ed.; Haward, R. N., Ed.; John Wiley & Sons: New York, 1973; pp 208 and 209.
(57) McCrum, N. G.; Read, B. E.; Williams, G. *Anelastic and Dielectric Effects in Polymeric Solids*, 2nd ed.; Dover: New York, 1991; pp 410–420.
(58) Cooper, T. M.; Stone, M. O.; Obermeier, K.; Crane, R.; Epling, R.; Tokarski, Z.; Natarajan, L. V. *Polym. Prepr. (Am. Chem. Soc., Div. Polym. Chem.)* **1993**, *34*, 598, 599.
(59) Man, H.-T.; Hyun, H. N. *Adv. Mater.* **1992**, *4*, 159–167.
(60) Van der Vorst, C. P. J. M.; Van Weedenberg, C. J. M. *SPIE Proc.* **1990**, *1337*, 246–254.
(61) Williams, M. L.; Landel, R. L.; Ferry, J. D. *J. Am. Chem. Soc.* **1955**, *77*, 3701–3707.
(62) Ferry, J. D. *Viscoelastic Properties of Polymers*, 3rd ed.; John Wiley and Sons: New York, 1980; pp 289–290.
(63) Ferry, J. D.; Grandine, L. D.; Fitzgerald, E. R. *J. Appl. Phys.* **1953**, *24*, 911–916.
(64) DeLaussus, P. T. In *Encyclopedia of Polymer Science and Engineering*; Wiley: New York, 1987; Vol. 16, pp 165–179.
(65) Fulcher, G. *J. Am. Ceram. Soc.* **1925**, *8*, 339–349.
(66) Ngai, K. L.; Rendell, R. W.; Rajagopal, A. K.; Teitler, S. *J. Chem. Phys.* **1989**, *91*, 8002, 8003.
(67) McKenna, G. B. In *Comprehensive Polymer Science: Polymer Properties*; Booth, C., Price, C., Eds.; Pergamon Press: New York, 1989; Vol. 2, pp 329–332.
(68) Burland, D. M.; Twieg, R. J.; Volksen, W.; Walsh, C. A. *SPIE Proc.* **1993**, *1852*, 186–197.
(69) Walsh, C. A.; Burland, D. M.; Lee, V. Y.; Miller, R. D.; Smith, B. A.; Twieg, R. J.; Volksen, W. *Macromolecules* **1993**, *26*, 3720–3722.
(70) Firestone, M. A.; Marks, T. J.; Ratner, M. A. Submitted for publication.

MA945010X